J Therm Anal Calorim (2012) 109:1321–1331
DOI 10.1007/s10973-011-1811-3

Thermal behaviors of *N*-pyrrolidine-*N*′-(2-chlorobenzoyl)thiourea and its Ni(II), Cu(II), and Co(III) complexes

Fatih M. Emen · Nevzat Külcü

Received: 27 April 2011 / Accepted: 18 July 2011 / Published online: 13 August 2011

Abstract The *N*-pyrrolidine-*N*′-(2-chlorobenzoyl)thiourea, HL, and their Ni(II), Cu(II), and Co(III) complexes (NiL_2, CuL_2, and CoL_3) have been synthesized and characterized. The thermal decomposition reactions of all the compounds have been investigated by DTA/TG combined systems. The mass spectroscopy technique has been used to identify the products during pyrolytic decomposition. The pyrolytic final products have been analyzed by X-ray powder diffraction method. After comparison of thermogravimetric and mass results of HL, NiL_2, CuL_2, and CoL_3, the decomposition mechanism of these compounds have been suggested. The thermal stability of the Ni(II) and Cu(II) complexes according to the thermogravimetric curves follows the sequence: $NiL_2 < CuL_2$. The values of the activation energy, E_a, have been obtained using model-free (Kissenger–Akahira–Sunose, KAS, Flyn–Wall–Ozawa, FWO, and Isoconversional) methods for all decomposition stages. The E_a versus the extent of conversion, α, plots show that the values of E_a varies as α. Thirteen kinetic model equations have been tested for selecting correct reaction models. The optimized value of E_a and Arrhenius factor, A, have been obtained using the best model equation. The thermodynamic functions (ΔH^*, ΔS^*, and ΔG^*) have been calculated using these values.

Keywords Benzoylthioureas · Thermal behavior · Thermal decomposition · Non-isothermal kinetics · Kinetic model

F. M. Emen (✉)
Department of Chemistry, Faculty of Arts and Science, Kirklareli University, 39160 Kirklareli, Turkey
e-mail: femen106@gmail.com

N. Külcü
Department of Chemistry, Faculty of Arts and Science, Mersin University, 33343 Mersin, Turkey

Introduction

The first benzoylthioureas were prepared from benzoylchloride, NH_4SCN, and amines by Dougles and Dains [1]. The use of *N*,*N*-disubstituted-*N*′-benzoylthioureas as ligands for transition-metal ions has received considerable attention because of their applications in separation processes [2–5]. Also, benzoylthiourea derivatives are widely used in a great number of applications such as in pharmaceutical industry for potential therapeutic agents as antibacterial [6, 7], anti-HIV [8], anticancer drugs [9], antidepressants [10] and antihyperlipidemic, antiallergic, antiparasitic, platelet antiaggregating, and antiproliferative activities [11]. The thiourea derivatives have been used extensively and commercially as herbicides, fungicides, and insecticides agents in the agrochemical industries [12, 13]. Recently, benzoylthiourea derivative complexes have been employed successfully as catalyst in the palladium-catalyzed Suzuki and Heck reactions because these ligands are thermally stable and insensitive to air and moisture [14–16].

The *N*-pyrrolidine-*N*′-(2-chlorobenzoyl)thiourea, HL, and its nickel Ni(II), copper Cu(II), and cobalt Co(III) complexes were synthesized and characterized in our previous study [17]. In this study, the thermal behavior and decomposition characteristics of these compounds have been investigated. The values of the activation energy, E_a, have been calculated by the KAS, FWO, and Isoconversional integral model-free equations [18–29]. As many as thirteen model equations have been tested for the best kinetic models giving the highest linear regression, the lowest standard deviation and giving the E_a values in good agreement with those calculated from model-free KAS and FWO methods. The optimized value of the E_a and A have been calculated using the best equation. Also, the other thermodynamic functions (ΔH^*, ΔS^*, and ΔG^*) have been obtained using these values.

Experimental

Preparation of ligand (HL) and its metal complexes

All chemicals used for preparation of the ligand and complexes were provided by Merck. The ligand and its metal complexes were synthesized according to the literature [17]. The solution of 2-chlorobenzoyl chloride (5×10^{-2} mol) in acetone (50 cm^3) was added dropwise to a suspension of potassium thiocyanate (5×10^{-2} mol) in acetone (30 cm^3). The reaction mixture was heated under reflux for 30 min, and then cooled down to room temperature. The solution of pyrrolidine (5×10^{-2} mol) in acetone (10 cm^3) was added, and the resulting mixture was stirred for 2 h. After the mixture was poured into hydrochloric acid (0.1 N, 300 cm^3), the precipitation in the solution was filtered and washed with distilled water. Then, the precipitation was purified by recrystallization from ethanol:dichloromethane mixture (1:1).

The metal acetate solutions (2.5×10^{-2} mol) in ethanol (30 cm^3) were added dropwise to the solution of the ligand to secure the ratio of metal:ligand 1:2 for Ni(II), Cu(II), and 1:3 for Co(III) with a small excess of ligand in dichloromethane (50 cm^3) at room temperature. The solid complexes were recrystallized from ethanol/dichloromethane mixture (1:1).

Instrumentals

The TG/DTA/DTG curves were recorded by a Shimadzu DTG-60H equipped with DTA and TG units. The thermal analysis system was used in the temperature range of 273–1450 K. The samples were placed in Pt crucibles, and α-Al_2O_3 was used as the reference material. Measurements were performed using a dynamic nitrogen furnace atmosphere at a flow rate of 50 mL min^{-1}. Different heating rates were chosen as 5, 10, and 15 °C min^{-1}, and the sample sizes vary in the mass range of 6–10 mg. Mass spectra were recorded with an Agilent 5975 C89 GC–MS spectrometer, along with EI techniques. Microanalyses were obtained using a Carlo Erba MOD 1106 instrument. X-ray powder diffraction analysis of the final residues were made with a Siemens F model diffractometer equipped with an X-ray generator, Phillips, PW-1010 model ranging from 20 to 40 kV and 6 to 50 mA while using a fine focus CuK_α radiation ($\lambda = 1.5406$ Å).

Results and discussion

N-pyrrolidine-*N*′-(2-chlorobenzoyl)thiourea, HL, and its Ni(II), Cu(II), and Co(III) complexes have been studied by thermogravimetric analysis from ambient temperature up to 1450 K under nitrogen atmosphere. The decomposition temperature range, DTA peak positions, percentage of mass losses, and evolved moieties of the decomposition reactions are summarized in Table 1.

Thermal decompositions

N-pyrrolidine-N′-(2-chlorobenzoyl)thiourea, HL

The TG/DTA/DTG curves of the HL obtained under N_2 (nitrogen) atmosphere within the temperature range of 278–1300 K are shown in Fig. 1.

Table 1 Thermoanalytical results of the decomposition reactions of HL, NiL_2, CuL_2, and CoL_3

Sample	Stage	DTA peak/K	TG temp. range/K	Mass loss/%		Evolved moiety
				Exper.	Theor.	
HL	I	455	431–475	22.00	21.95	–HNCS
	II	499	475–725	78.00	78.05	$-C_{11}H_{12}NOCl$
NiL_2	I	523	508–547	33.90	35.30	$-C_{11}H_{12}NOCl$
	II	566	547–708	33.50	35.00	$-C_{11}H_{12}NOCl$
	III	–	708–1300	19.50	16.35	[a]
	Residue		–	13.10	13.35	Ni_3S_2
CuL_2	I	433	300–581	33.70	34.90	$-C_{11}H_{12}NOCl$
	II	595	549–709	35.40	34.90	$-C_{11}H_{12}NOCl$
	III	–	709–1426	14.94	14.26	[a]
	Residue		–	15.96	15.94	CuS
CoL_3	I	520	485–548	23.40	24.30	$-C_{11}H_{12}NOCl$
	II	588	548–757	47.40	48.59	$-2C_{11}H_{12}NOCl$
	III	–	757–1180	19.08	16.98	[a]
	Residue		–	10.12	10.13	Co_9S_8

[a] Unknown product

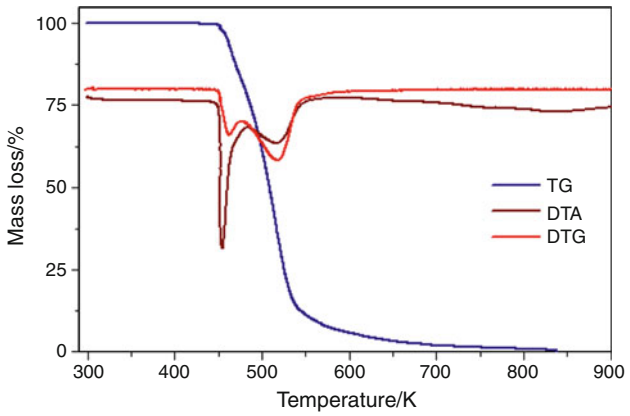

Fig. 1 DTA/TG/DTG curves of HL

It can be observed from the TG and DTG curves that the decomposition process of the HL takes place in two stages. The first decomposition stage occurs in the temperature range of 431–475 K. In this step, the elimination of HNCS group resulted in an experimental mass loss of 22.00% (Calc.:21.95%). The second decomposition is observed in the temperature range of 475–725 K along with a mass loss of 78.00% (Calc.:78.05%). At this stage, $C_{11}H_{12}NOCl$ molecule was broken up and turned into the gas products. The DTA curve shows two endothermic peaks. The first between 431 and 475 K with a minimum at 455 K and the second between 475 and 585 K with a minimum at 499 K, respectively. The first peak corresponds to melting and then decomposition of the HL. The melting and the decomposition of the HL take place at the same temperature range. The second one corresponds to decomposition of the HL. The maximum rate of mass loss occurs at 450 and 499 K, respectively, as indicated by the minimas of the DTG curve. The suggested decomposition mechanism advanced on the basis of thermal analysis data correlated to the mass spectral measurements (see Fig. 2) is illustrated in Scheme 1.

Fig. 2 Mass spectra of HL

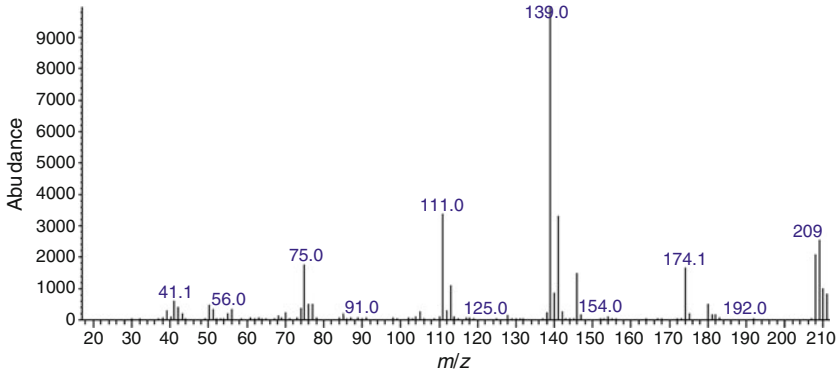

Scheme 1 The mechanism for the decomposition reaction of HL

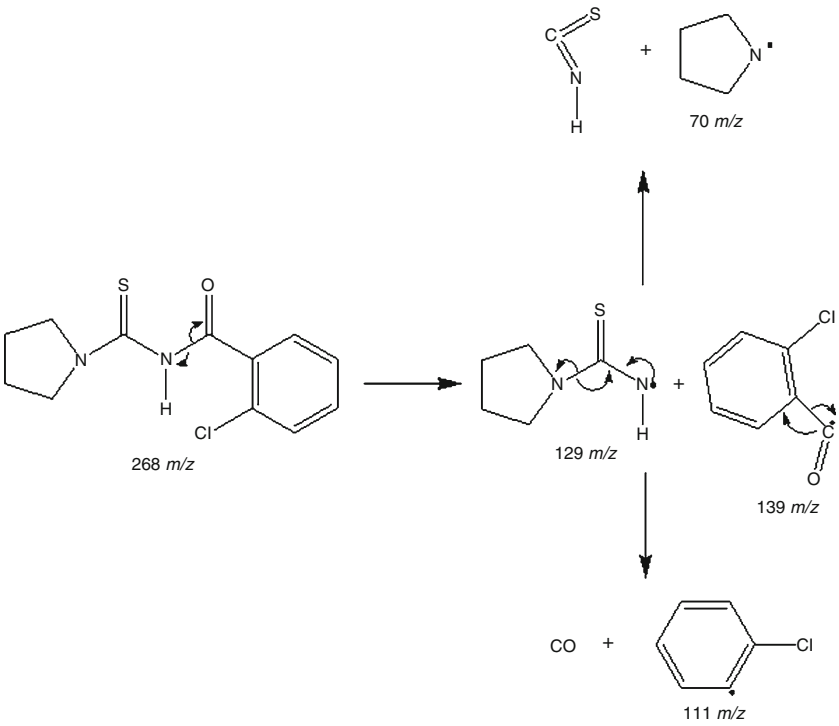

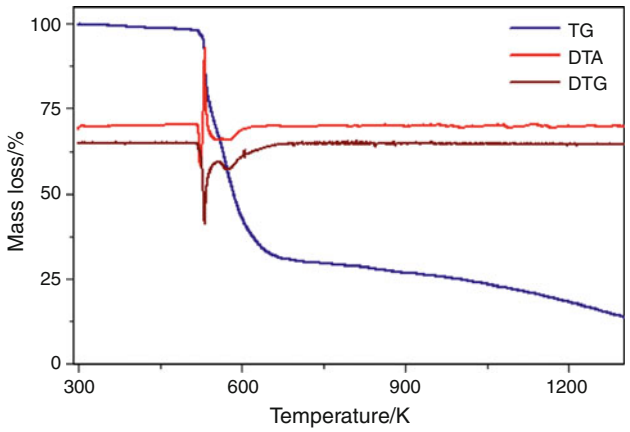

Fig. 3 DTA/TG/DTG curves of NiL_2 complex

Bis-[N-pyrrolidine-N′-(2-chlorobenzoyl)thioureato]nickel(II) complex, NiL_2

NiL_2 complex undergoes decomposition in three stages. In the first stage, $C_{11}H_{12}NOCl$ molecule left out NiL_2 complex in the temperature range of 508–547 K with a mass loss 33.90% (Calc.:35.00%). Thus, the intermediate product at the first stage was determined as $C_{13}H_{12}N_3OS_2ClNi$. The second decomposition stage at which the $C_{11}H_{12}NOCl$ left out this intermediate product was observed in the temperature range of 547–708 K. The mass loss of this elimination was about 33.50% (Calc.:35.30%). The intermediate yield determined in the second stage was $Ni(SCN)_2$. At the final stage which occured in between 708 and 1300 K, some unknown products left out. After all these eliminations, it was determined that the final product was Ni_3S_2 (JCPDF File No: 76-1870) with a mass loss of 13.10% (Calc.:13.35%) and with a yellowish-bronze color. There are two endothermic peaks observed in the DTA curve: the first one is in between 516 and 532 K with a minimum peak point at 523 K, the second one is in between 532 and 608 K with a minimum peak point at 566 K, respectively. The first endothermic effect corresponds to the melting point of NiL_2 complex at 523 K. The rate of the mass loss is found to be maximum at 533 and 578 K for the first and second stages of the decomposition, respectively, as indicated by the minimas of the DTG curve. The DTA/TG/DTG curves of the NiL_2 complex are presented in Fig. 3. The decomposition mechanism of the NiL_2 complex is suggested with the help of TG and XRD results and is illustrated in Scheme 2. The X-ray diffraction pattern of the end product as Ni_3S_2 is shown in Fig. 4.

Bis-[N-pyrrolidine-N′-(2-chlorobenzoyl) thioureato]copper(II) complex, CuL_2

The TG/DTA/DTG curves of CuL_2 complex are shown in Fig. 5. The TG curve indicates that it is thermally stable up to 300 K, and the decomposition starts beyond this temperature as shown by the first mass loss stage in the TG curve. At the first stage which occurs in between 300 and 581 K, CuL_2 decomposes with a mass loss of 33.70% (Calc.:34.90%). In the second stage, the mass loss of 35.40% (Calc.:34.90%) is observed in between 549 and 709 K. The $C_{11}H_{12}NOCl$ group leaves out not only in the first stage but also in the second stage. In the third stage observed in between 709 and 1426 K, some unknown products break off. The final product with black color was identified by X-ray diffraction pattern shown in Fig. 6 as CuS (JCPDS File No: 65-7111). In the DTA curve of CuL_2 complex, the exothermic peak is observed as well as the endothermic peak. The exothermic peak lies in between 417 and 480 K with a peak maxima at 433 K and the endothermic one takes place in between 550 and 650 K with a minimum peak point at 595 K, respectively. These endothermic and exothermic peaks correspond to the decomposition of the CuL_2 complex. In contrast to the NiL_2 complex, the endothermic peak which corresponds to the melting point of the CuL_2 complex is not observed in DTA curve, because the decomposition and the melting of the CuL_2 complex take place at the same temperature range and the time. The maximum rates of mass loss as indicated by the minimas of the DTG curve are found to be at 470 K for the first stage and 600 K for the second one. The expected decomposition mechanism is given in Scheme 2.

Scheme 2 The mechanism for the decomposition reaction of NiL_2, CuL_2, and CoL_3 complexes

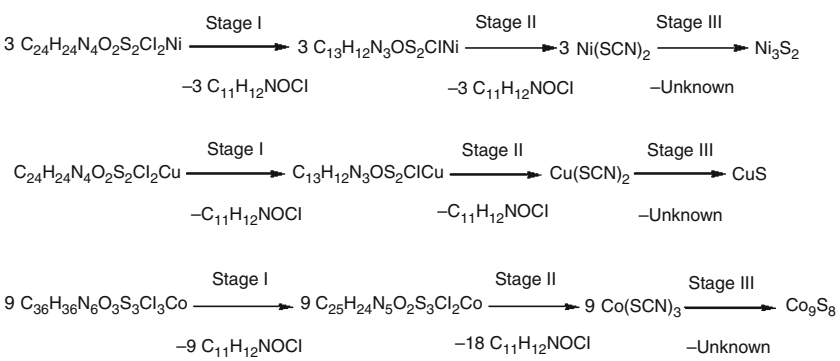

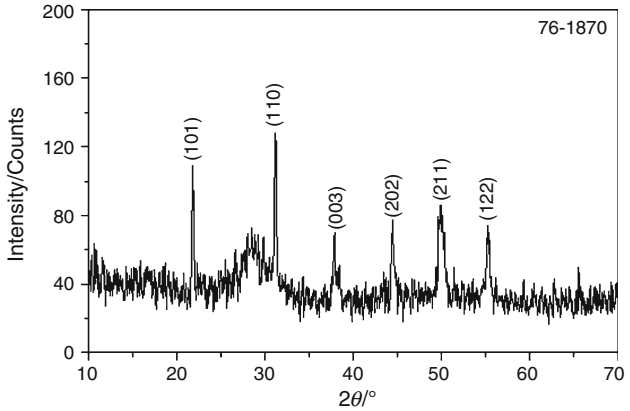

Fig. 4 X-ray powder diffraction pattern of Ni_3S_2 (JCPDS File No: 76-1870)

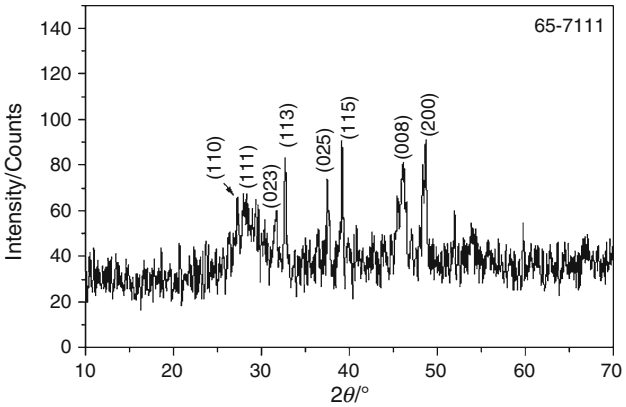

Fig. 6 X-ray powder diffraction pattern of CuS (JCPDS File No: 65-7111)

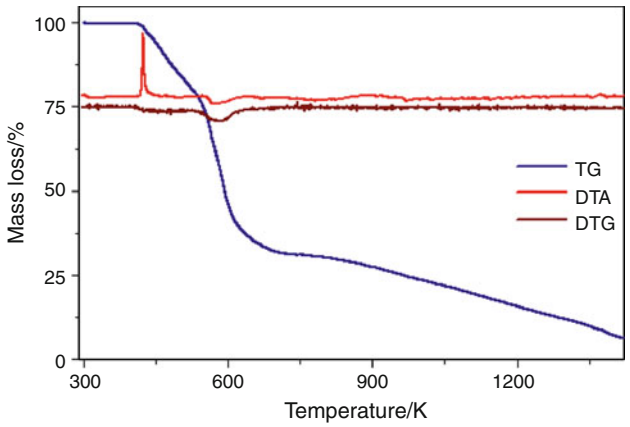

Fig. 5 DTA/TG/DTG curves of CuL_2 complex

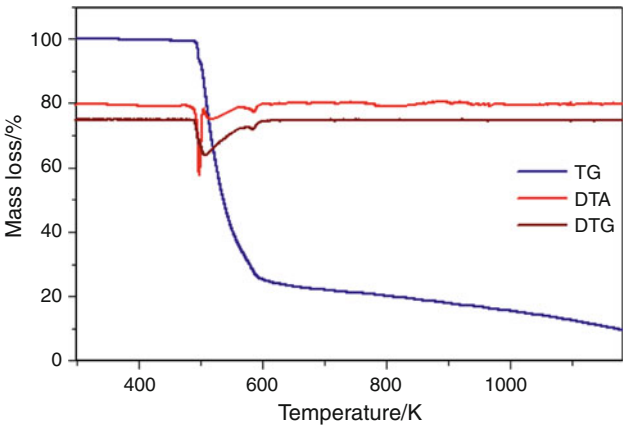

Fig. 7 DTA/TG/DTG curves of CoL_3 complex

Tris-[N-pyrrolidine-N′-(2-chlorobenzoyl) thioureato]cobalt(III), CoL_3

It was determined from the TG and DTG curves shown in Fig. 7 that the CoL_3 complex decomposes in three stages. In the first stage which occured in between 485 and 548 K along with 23.40% (calc. 24.30%) mass loss because of the elimination of $C_{11}H_{12}NOCl$ group from the CoL_3 complex. The second decomposition stage takes place in the temperature range of 548–757 K along with the mass loss of 47.40% (calc. 48.59%). The elimination of two moles of $C_{11}H_{12}NOCl$ group occurs in this stage. At the final decomposition stage which occurred in the temperature range of 757–1180 K, the mass loss is 19.08% (calc. 16.98%) because of the elimination of some unknown products. The X-ray diffraction studies show that the residual black solid was Co_9S_8 (JCPDS File No: 65-6801) which corresponds to a mass of 10.12% (calc. 10.13%) of the complex (see Fig. 8). The expected decomposition mechanism is given in Scheme 2. There are three endothermic peaks observed in the DTA curve: the first one is in

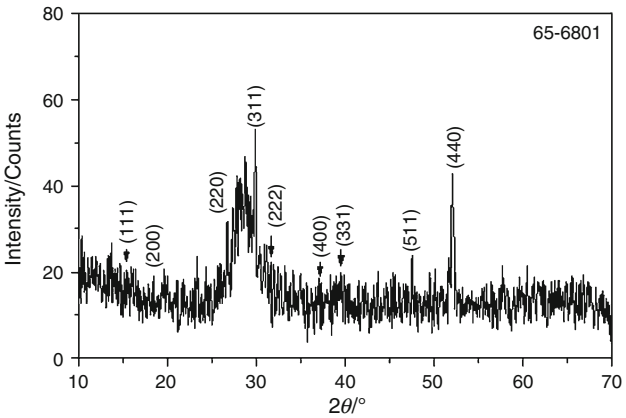

Fig. 8 X-ray powder diffraction pattern of Co_9S_8 (JCPDS File No: 65-6801)

between 476 and 505 K with a minimum peak point at 500 K, the second one is in between 505 and 568 K with a minimum peak point at 520 K, and the third one is in between 564 and 603 K with a minimum peak point at 588 K. The first endothermic effect corresponds to the

melting point of the CoL_3 complex at 500 K. The other endothermic peaks correspond to the decomposition of the CoL_3 complex. The rate of the mass loss is found to be maximum at 508 and 587 K for the first and second stages of the decomposition, respectively, as indicated by the minimas of the DTG curve.

Kinetic analysis

The non-isothermal thermogravimetry is used to determine apparent kinetic parameters of the thermal decomposition reactions (the reaction order, n, the activation energy, E_a, and frequency factor, A).

In our kinetic study for HL and its metal complexes such as NiL_2, CuL_2, and CoL_3 compounds, the KAS, FWO, and Isoconversional equations [20–24] were used to determine the activation energy, E_a, of the decomposition reactions, α, for the conversion degree varying in the range of 0.1–1.0 in a step of 0.1.

The kinetic equations are described as following:

KAS equation:

$$\ln\frac{\beta}{T^2} = \ln\frac{AR}{g(\alpha)E_a} - \frac{E_a}{RT} \tag{1}$$

FWO equation:

$$\ln\beta = \left(\frac{AE_a}{Rg(\alpha)}\right) - 5.3305 - 1.05178\frac{E_a}{RT} \tag{2}$$

Isoconversional equation:

$$-\ln t = \ln\frac{A}{g(\alpha)} - \frac{E_a}{RT} \tag{3}$$

where β is the heating rate (K min^{-1}), A is the pre-exponential factor (min^{-1}), R is the gas constant (8.314 J mol^{-1} K^{-1}), and T is the absolute temperature, K.According to the aforementioned equations, the plots of $\ln\beta$ versus $1/T$, $\ln\beta/T^2$ versus $1/T$ and $-\ln t$ versus $1/T$ give parallel lines for each α value. The activation energies can be calculated from the slopes of every straight line with linear correlation coefficient, r. The activation energies, E_a, of the decomposition process calculated under the non-isothermal conditions are given in Table 2.

KAS and FWO equations have been re-arranged to find the kinetic triplet, E_a, A, $g(a)$ [30–32]. These methods are known as "composite method I" and "composite method II" in literature [33, 34].

Modeling KAS equation (Composite Method I, C.M I):

$$\ln\frac{g(\alpha)}{T^2} = \ln\frac{AR}{\beta E_a} - \frac{E_a}{RT} \tag{4}$$

Modeling FWO equation (Composite Method II, C.M II):

$$\ln g(\alpha) = \left(\frac{AE_a}{\beta R}\right) - 5.3305 - 1.05178\frac{E_a}{RT}. \tag{5}$$

The plots of $\ln[g(\alpha)/T^2]$ versus $1/T$ (in model fitting with KAS method) and $\ln g(\alpha)$ versus $1/T$ (in model fitting with FWO method) give parallel lines for each α value at single β value. Different kinetic model functions are given in Table 3. The E_a and A values have been calculated for each model functions, $g(\alpha)$. The best kinetic model function giving activation energies in good agreement with those obtained using model-free KAS and FWO methods and also has the highest regression analysis and the lowest standard deviation. The changes of the entropy, ΔS^*, enthalpy, ΔH^*, and Gibbs free energy, ΔG^*, for the activated complex can be calculated using the thermodynamic equations;

Table 2 The values of the activation energy, E_a, of the decomposition processes

Compounds	Stage	FWO method E_a/kJ mol^{-1}	KAS method E_a/kJ mol^{-1}	Isoconversional method E_a/kJ mol^{-1}
HL	I	*84.99*	*81.31*	103.61
	II	*51.61*	*45.05*	59.27
NiL_2	I	127.80	125.43	133.00
	II	96.44	88.42	95.05
	III	34.66	16.95	25.59
CuL_2	I	131.79	131.32	132.76
	II	101.63	96.43	98.89
	III	59.84	42.85	50.10
CoL_3	I	112.77	110.06	110.06
	II	98.51	94.04	94.77
	III	86.06	76.88	81.68

Table 3 Different kinetic model functions for evaluation of the kinetic

	Reaction model	Code	$g(\alpha)$
1	Power law	P4	$\alpha^{1/4}$
2	Power law	P3	$\alpha^{1/3}$
3	Power law	P2	$\alpha^{1/2}$
4	Power law	P2/3	$\alpha^{3/2}$
5	One-dimensional diffusion	D1	α^2
6	Mampel (First order)	F1	$-\ln(1-\alpha)$
7	Avrami-Erofeev	A4	$-[\ln(1-\alpha)]^{1/4}$
8	Avrami-Erofeev	A3	$-[\ln(1-\alpha)]^{1/3}$
9	Avrami-Erofeev	A2	$-[\ln(1-\alpha)]^{1/2}$
10	Three-dimentional diffusion	D3	$[1-(1-\alpha)^{1/3}]^2$
11	Contracting sphere	R3	$1-(1-\alpha)^{1/3}$
12	Contracting cylinder	R2	$1-(1-\alpha)^{1/2}$
13	Two-dimensional diffusion	D2	$(1-\alpha)\ln(1-\alpha)+\alpha$

$$A = (kT_{\text{avg.}}/h)e^{\Delta S^*/R} \quad (6)$$

$$\Delta H^* = E_a - RT_{\text{avg.}} \quad (7)$$

$$\Delta G^* = \Delta H^* - T_{\text{avg.}}\Delta S^* \quad (8)$$

where E_a is the activation energy which is calculated from slope of modeling method curves for the most suitable model, k is the Boltzmann constant, h is the planck's constant, and $T_{\text{avg.}}$ is average reaction temperature.

The dependencies of E_a versus α are very important for determination of the multi-step kinetics. A significant variation of E_a with α indicates that decomposition process is kinetically complex [30–32].

The activation energies, E_a, for all the compounds were calculated using the above mentioned three model-free methods and showed a similar tendency for the α-dependence in each stage. The E_a versus α for HL based on the FWO, KAS, and Isoconversional methods are shown for decomposition stage one and stage two in Fig. 9a and b, respectively. In stage I, the E_a values calculated using the Isoconversional method are greater than those calculated using either FWO or KAS methods. The results of the FWO and KAS methods are quite similar. The average E_a values are 84.99, 81.31, and 103.61 kJ mol^{-1} calculated using the FWO, KAS, and Isoconversional methods, respectively. Further, it seems in Fig. 9a that the E_a decreases with two different slopes depending on the α. Therefore, it is concluded that the decomposition occurs at least in two steps.

In stage II, the activation energies of the HL calculated using the FWO, KAS, and Isoconversional methods show quite similar behaviors. The E_a values obtained using the Isoconversional method are higher than those of obtained using FWO and KAS methods similar to the stage I. However, in contrast to the stage I, the E_a values remain relatively constant in the conversion degree range of 0.1–0.9 and decrease drastically at $\alpha = 0.9$. Therefore, it is concluded that there is only one dominant kinetic process. The E_a values are 51.61, 45.04, and 59.27 kJ mol^{-1} calculated in the α range of 0.1–0.9 using the FWO, KAS, and Isoconversional methods (see Fig. 9b).

The α dependent E_a of NiL_2 complex calculated using the FWO, KAS, and Isoconversional methods are shown for all decomposition stages in Fig. 10a, b, c, respectively. The activation energy values of NiL_2 complex calculated by the FWO, KAS, and Isoconversional methods show similar α-dependent behavior for each stage.

In stage I, the E_a values calculated using the Isoconversional method are slightly higher than those calculated using the FWO and KAS methods. The E_a increases up to $\alpha = 0.2$. Finally, for $\alpha > 0.9$, the E_a increases again (see Fig. 10a). The activation energy decreases as the

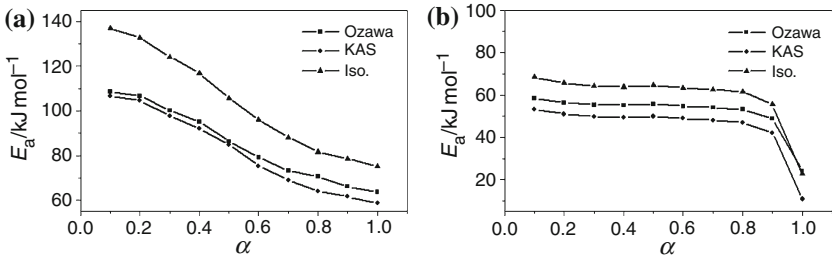

Fig. 9 The E_a versus α for HL based on Ozawa, KAS, and Isoconversional methods: **a** the first decomposition stage and **b** the second decomposition stage

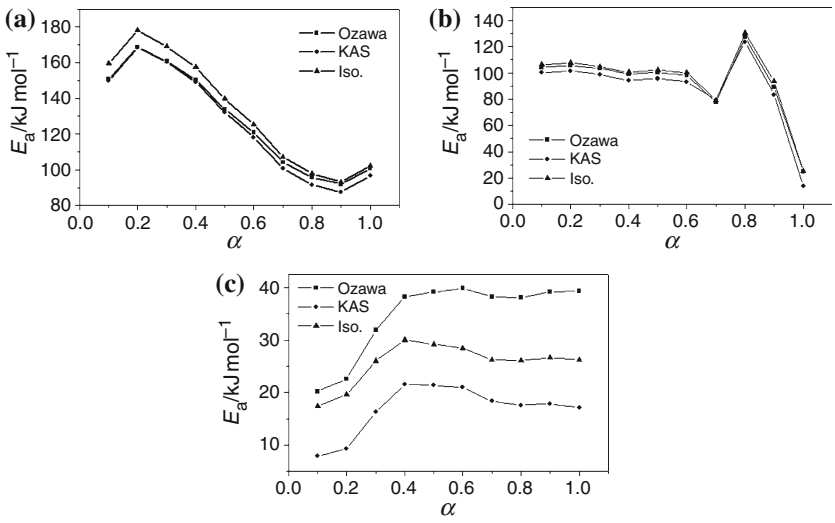

Fig. 10 The E_a versus α for NiL_2 complex based on Ozawa, KAS, and Isoconversional methods: **a** the first decomposition stage, **b** the second decomposition stage, and **c** the third decomposition stage

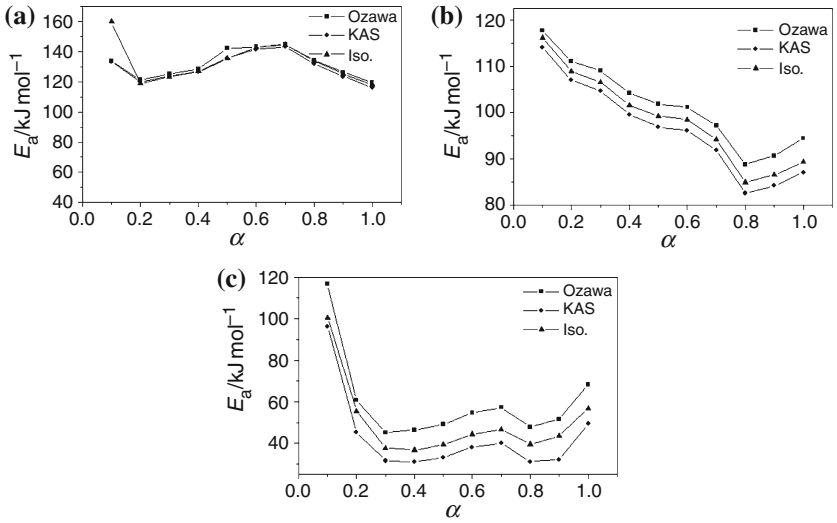

Fig. 11 The E_a versus α for CuL_2 complex based on Ozawa, KAS, and Isoconversional methods: **a** the first decomposition stage, **b** the second decomposition stage, and **c** the third decomposition stage

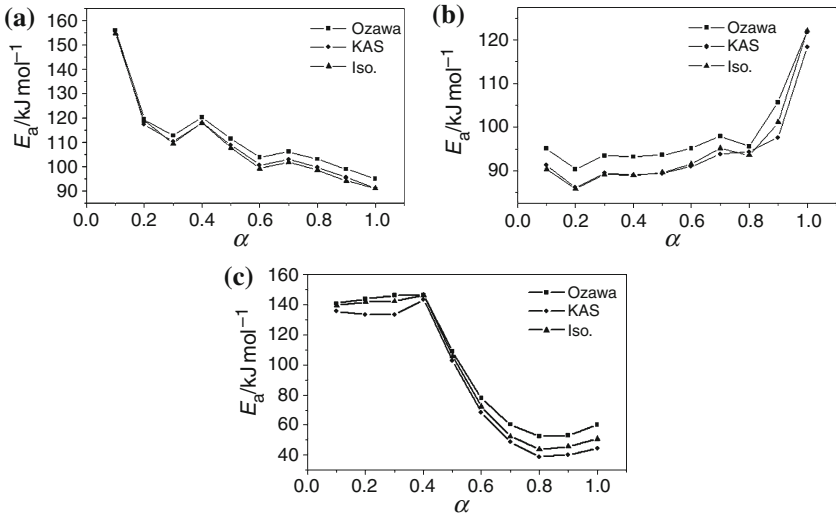

Fig. 12 The E_a versus α for CoL_3 complex based on Ozawa, KAS, and Isoconversional methods: **a** the first decomposition stage, **b** the second decomposition stage, and **c** the third decomposition stage

conversion degree, α, increases indicating that the decomposition contains at multi-steps. The average E_a values are 127.80, 125.43, and 128.75 kJ mol^{-1} for the FWO, KAS, and Isoconversional methods, respectively.

In stage II, the E_a values calculated by the FWO, KAS, and Isoconversional methods are quite similar to each other and remain approximately constant up to $\alpha = 0.6$ beyond which they show a slight decrease up to $\alpha = 0.7$, a sharp increase between $0.7 \leq \alpha \leq 0.8$, and a sharp decrease afterwards (see Fig. 10b). Therefore, it was concluded that the decomposition contains only one step up to $\alpha = 0.6$, but between $0.6 \leq \alpha \leq 1.0$ the decomposition contains more than one step. The average E_a values are 96.44, 88.42, and 93.30 kJ mol^{-1} for the FWO, KAS, and Isoconversional methods, respectively.

In stage III, in contrast to stages I and II, E_a values calculated using the FWO, KAS, and Iso-conversional methods differ from each other. The E_a values calculated by the FWO method are greater than those calculated by the Isoconversional method which, in turn, are greater than the values obtained by the KAS method. However, all of the E_a values calculated by these three methods show quite similar α dependency: the E_a values increase up to $\alpha = 0.4$ and approximately remain stable at $\alpha \geq 0.4$ (see Fig. 10c). The average E_a values are 34.66, 16.95, and 75.73 kJ mol^{-1} calculated by the FWO, KAS, and Isoconversional methods, respectively.

The α dependent E_a of CuL_2 complex calculated using the FWO, KAS, and Isoconversional methods are shown for all decomposition stages in Fig. 11a, b, c, respectively. The E_a values of CuL_2 complex calculated by the FWO, KAS and Isoconversional methods show similar α-dependent behavior for each stage.

In stage I, the E_a values calculated using these three methods are quite similar except for the one calculated by Isoconversional method at $\alpha = 0.1$. The E_a values slightly

Table 4 The activation energy, E_a, values which calculated Composite Methods

Compounds	Stage	Model	Composite model I			Composite model II		
			R^2	SD	E_a/kJ mol^{-1}	R^2	SD	E_a/kJ mol^{-1}
HL	I	A2	0.980	1.4	91.10	0.990	5.03	95.08
	II	A2	0.985	4.85	47.92	0.985	0.49	63.88
	I	A2	0.968	14.89	131.69	0.962	21.82	138.90
NiL_2	II	A3	0.959	19.20	104.25	0.987	17.09	111.03
	III	A2	0.987	0.42	34.54	0.990	8.3	41.76
	I	A2	0.970	1.06	142.7	0.985	0.73	143.68
CuL_2	II	A2	0.982	6.13	100.11	0.978	9.82	106.92
	III	A2	0.980	5.2	49.02	0.965	2.54	64.5
	I	A2	0.980	25.81	120.7	0.980	4.23	129.77
CoL_3	II	A2	0.960	5.58	109.84	0.972	7.5	119.47
	III	A2	0.981	3.82	84.82	0.960	8.29	98.21

Table 5 The thermodynamic parameters for all decomposition stages

Compounds	Stage	Method	Model	E_a/kJ mol^{-1}	ln A/kJ mol^{-1}	ΔH*/kJ mol^{-1}	ΔS*/J mol^{-1}	ΔG*/kJ mol^{-1}
HL	I	C.M I	A2	91.10	9.52	87.32	−200.72	178.65
		C.M II	A2	95.08	7.87	91.30	−214.42	188.86
	II	C.M I	A2	47.92	9.63	43.77	−200.57	191.38
		C.M II	A2	63.88	8.75	59.73	−207.89	163.47
NiL_2	I	C.M I	A2	131.69	9.88	127.34	−198.88	231.35
		C.M II	A2	138.90	8.575	134.55	−209.73	244.24
	II	C.M I	A3	104.25	9.54	99.54	−202.36	214.08
		C.M II	A3	111.03	7.545	106.32	−218.95	230.25
	III	C.M I	A2	34.54	10.87	26.22	−196.04	222.26
		C.M II	A2	41.76	8.46	33.45	−216.08	249.53
CuL_2	I	C.M I	A2	142.7	9.52	139.10	−200.30	225.83
		C.M II	A2	143.68	7.61	140.08	−216.18	233.69
	II	C.M I	A2	100.11	9.57	95.16	−202.53	215.36
		C.M II	A2	106.92	7.893	101.97	−216.47	230.77
	III	C.M I	A2	49.02	10.13	41.12	−202.02	233.04
		C.M II	A2	64.5	8.688	56.60	−213.75	259.66
CoL_3	I	C.M I	A2	120.7	9.35	116.37	−203.24	222.05
		C.M II	A2	129.77	7.279	125.45	−220.46	240.09
	II	C.M I	A2	109.84	9.58	104.95	−202.35	223.93
		C.M II	A2	119.47	7.682	114.58	−218.13	242.84
	III	C.M I	A2	84.82	10.39	76.51	−200.03	276.54
		C.M II	A2	98.21	8.968	89.90	−211.85	301.75

increase as α increases up to 0.7 and then starts to decrease (see Fig. 11a). Therefore, it was concluded that the decomposition occurs at multi-steps. The average E_a values are 131.79, 131.32, and 132.76 kJ mol^{-1} for the FWO, KAS, and Isoconversional methods, respectively.

In stage II, the E_a values calculated using the three methods slightly differ from each other whereas they show quite similar α-dependent behavior. The E_a values decrease with increasing α up to α = 0.8 (see Fig. 11b), and then start to increase, indicating that the decomposition occurs in more than one step. The average E_a values are 101.60, 96.45, and 98.90 kJ mol^{-1} for FWO, KAS, and Isoconversional methods, respectively.

In stage III, the E_a values calculated using the three methods slightly differ from each other whereas they show quite similar α-dependent behavior, the same as stage II.

The E_a values decrease very fast with increasing α up to $\alpha = 0.3$ and then increase quite slightly up to $\alpha = 0.7$ (see Fig. 11c). The average E_a values are 59.85, 42.85, and 50.93 kJ mol^{-1} for the FWO, KAS, and Isoconversional methods, respectively.

The α-dependent E_a of CoL_3 complex calculated by the three methods is shown for all decomposition stages in Fig. 12a, b, c.

In stage I, the E_a values calculated using the FWO, KAS, and Isoconversional methods are quite similar. The E_a values decrease up to $\alpha = 0.3$ and then increases. Finally, the E_a values decrease in the range of $0.4 \leq \alpha \leq 1.0$ (see Fig. 12a). Therefore, it was concluded that the decomposition occurs at multi-steps. The average E_a values are 112.77, 110.06, and 110.96 kJ mol^{-1} for the FWO, KAS, and Isoconversional methods, respectively.

In stage II, the E_a values calculated using the FWO method are greater than those calculated using the KAS and Isoconversional methods while they show quite similar α-dependent behavior. The E_a values decrease with increasing α up to $\alpha = 0.1$, and then slightly increase as α increases up to 0.8. Finally, the E_a values increase very fast in the range of $0.8 \leq \alpha \leq 1.0$ (see Fig. 12b). Therefore, it is concluded that the decomposition occurs in more than one step. The average E_a values are 98.51, 94.04, and 95.77 kJ mol^{-1} for the FWO, KAS, and Isoconversional methods, respectively.

In stage III, the E_a values calculated by the three methods slightly differ from each other while they show quite similar α-dependent behavior. The E_a values remain stable up to $\alpha = 0.4$, and then decrease very fast with increasing α up to $\alpha = 0.8$, beyond which they remain more or less constant (see Fig. 12c). Therefore, it was concluded that the decomposition occurs only in one step up to $\alpha = 0.4$, but it contains multi-steps in the range $0.4 \leq \alpha \leq 1.0$. The average E_a values are 88.06, 76.88, and 81.68 kJ mol^{-1} for the FWO, KAS, and Isoconversional methods, respectively.

The kinetic parameters (E_a and A) can be also obtained using re-arranged KAS and FWO equations. The reaction models have been investigated using thirteen kinetic model equations, and the most suitable models have been selected. General Integral Isoconversional equation which can be seen in Eq. 3 is only applicable to isothermal data [30]. This equation is not examined in the model-fitting studies. The E_a values, standard deviations, SD, and regression analysis, r^2, values which calculated with Composite Methods are given in Table 4. The best model equations have been determined as A2 and A3. These model equations correspond to nucleation and growth mechanism [30, 31]. The other thermodynamic parameters which have been calculated from the best model equations are presented in Table 5.

The activation energies of NiL_2 and CuL_2 complexes are expected to increase proportionally to the decrease in their ionic radius (r^{2+}_{Ni}=72 pm, r^{2+}_{Cu}=70 pm) [35]. NiL_2 and CuL_2 complexes have a square-planar geometry and show similar decomposition steps. A smaller size of Cu(II) permits a closer approach of the ligand as compared to Ni(II). Hence, the E_a value for the CuL_2 complex is higher than that of NiL_2 complex [36, 37]. The same behaviors are also true for the E_a values of the second and third stages with respect to the FWO, KAS, and Isoconversional methods. The thermal stability of the CuL_2 complex is greater than that of the NiL_2 complex according to the TG curves.

Conclusions

Thermal behavior of *N*-pyrrolidine-*N*′-(2-chlorobenzoyl)-thiourea, HL, and their Ni(II), Cu(II), and Co(II) metal complexes were studied by DTA/TG/DTG analysis under nitrogen atmosphere in the temperature range of 298–1450 K. The final products were identified as Ni_3S_2, $Cu_{1.96}S$, and Co_4S_3 by XRD analysis. The pyrolytic decomposition mechanism of the HL, NiL_2, CuL_2, and CoL_3 compounds were suggested depending on the thermogravimetric and mass results. The suggested thermal decomposition mechanism of *N*-pyrrolidine-*N*′-(2-chlorobenzoyl)thiourea and its metal complexes are summarized in Schemes 1 and 2. The values of the activation energy, E_a, of the thermal decomposition reactions were calculated by the FWO, KAS, and Isoconversional methods for all decomposition stages. The E_a *vs* α graphics of all compounds show that the E_a varies differently in each stages of every compounds. Therefore, it is concluded that the decompositions contain multi-step process. The thirteen kinetic model equations have been examined for selecting the best model-fitting equations. The optimized value of E_a and A have been calculated using the best model equation. The ΔH^*, ΔS^*, and ΔG^* have been obtained using these values.

Acknowledgements The authors thank to Dr. Selma Erat (ETH-Zurich, Switzerland) and Prof. Dr. Murat Ozer for their helpful discussions.

References

1. Douglass IB, Dains FB. Some derivatives of benzoyl and furoyl isothiocyanates and their use in synthesizing heterocyclic compounds. J Am Chem Soc. 1934;56:719–21.
2. Schuster M. Zur chromatographie von metallchelaten, XVI. Dünnschichtchromatographie von *N*,*N*-dialkyl-*N*′-thiobenzoylthioharnstoff-chelaten. Fresenius Z Anal Chem. 1986;324:127–9.
3. Konig KH, Schuster M, Schneeweis G, Steinbrech B. Zur chromatographie von metallchelaten, XIV. Dünnschicht-chromatographie von *N*,*N*-dialkyl-*N*′-benzoylthioharnstoff-chelaten. Fresenius Z Anal Chem. 1984;319:66–9.

4. Schuster M, Kugler B, Konig KH. The chromatography of metal chelates, XIX. Influence of the acyl substituents on the chromatographic properties of acylthiourea chelates. Fresenius J Anal Chem. 1990;338:717–20.
5. Konig KH, Schuster M, Steinbrech B, Schneeweis G, Schlodder R. *N*,*N*-dialkyl-*N*′-benzoylthioharnstoffe als selective extractionsmittel zur abtrennung und anreicherung von platinmetallen. Fresenius Z Anal Chem. 1985;321:457–60.
6. Arslan H, Duran N, Sahin NO, Kulcu N. Thermal behaviour and antimicrobial activity of novel series of benzoylthiourea derivatives. Asian J Chem. 2006;18:1710–8.
7. Arslan H, Duran N, Borekci G, Ozer CK, Akbay C. Antimicrobial activity of some thiourea derivatives and their nickel and copper complexes. Molecules. 2009;14:519–27.
8. Venkatachalam TK, Mao C, Uckun FM. Effect of stereochemistry on the anti-HIV activity of chiral thiourea compounds. Bioorg Med Chem. 2004;12:4275–84.
9. Sacht C, Datt MS, Otto S, Roodt A. Chiral and achiral platinum(II) complexes for potential use as chemotherapeutic agents: crystal and molecular structures of *cis*-$[Pt(L^1)_2]$ and $[Pt(L^1)Cl(MPSO)]$ [HL^1 = *N*,*N*-diethyl-*N*′-benzoylthiourea]. J Chem Soc Dalton Trans. 2000;5:727–733.
10. Ozer CK, Arslan H, Van Derveer D, Külcü N. Synthesis and characterization of *N*-(arylcarbamothioyl)-cyclohexanecarboxamide derivatives: the crystal structure of *N*-(naphthalen-1-ylcarbamothioyl)cyclohexanecarboxamide. Molecules. 2009;14:655–66.
11. Sun CW, Huang H, Feng M, Shi XL, Zhang XD, Zhou P. A novel class of potent influenza virus inhibitors: polysubstituted acylthiourea and its fused heterocycle derivatives. Bioorg Med Chem Lett. 2006;16:162–6.
12. Arslan H, Kulcu N, Florke U. Synthesis and characterization of copper(II), nickel(II) and cobalt(II) complexes with novel thiourea derivatives. Trans Met Chem. 2003;28:816–19.
13. Binzet G, Arslan H, Florke U, Kulcu N, Duran N. Synthesis, characterization and antimicrobial activities of transition metal complexes of *N*,*N*-dialkyl-*N*′-(2-chlorobenzoyl)thiourea derivatives. J Coord Chem. 2006;59:1395–406.
14. Yang D, Chen YC, Zhu NY. Sterically bulky thioureas as air and moisture stable ligands for Pd-catalyzed Heck reactions of aryl halides. Org Lett. 2004;6:1577–80.
15. Mingji D, Liang B, Wang C, You Z, Xiang J, Dong G, Chen J, Yang Z. A novel thiourea ligand applied in the Pd-catalyzed Heck, Suzuki and Suzuki carbonylative reactions. Adv Synth Catal. 2004;346(13–15):1669–73.
16. Dai M, Liang B, Wang C, Chen J, Yang Z. Synthesis of a novel C_2-symmetric thiourea and its application in the Pd-catalyzed cross-coupling reactions with arenediazonium salts under aerobic conditions. Org Lett. 2004;6(2):221–4.
17. Emen MF, Arslan H, Kulcu N, Florke U, Duran N. Synthesis, characterization and antimicrobial activities of some metal complexes with *N*′-(2-chloro-benzoyl)thiourea ligands: the crystal structure of fac-$[CoL_3]$ and cis-$[PdL_2]$. Pol J Chem. 2005; 79:1615–26.
18. Cilgi GK, Cetisli H. Thermal decomposition kinetics of aluminum sulfate hydrate. J Therm Anal Calorim. 2009;98:855–61.
19. Kücük F, Yildiz K. The decomposition kinetics of mechanically activated alunite ore in air atmosphere by thermogravimetry. Thermochim Acta. 2006;448:107–10.
20. Ozawa T. A new method of analyzing thermogravimetric data. Bull Chem Soc Jpn. 1965;38:1881–6.
21. Kissinger HE. Reaction of peak temperature with heating rate in different thermal analysis. J Res Nat Bur Stand. 1956;57:217–21.
22. Kissinger HE. Reaction kinetics in differential thermal analysis. Anal Chem. 1957;29:1702–6.
23. Akahira T, Sunose T. Joint convention of four electrical institutes. Res Rep Chiba Inst Technol. 1971;16:22–31.
24. Simon P. Isoconversional methods; fundamentals, meaning and application. J Therm Anal Calorim. 2004;76:123–32.
25. Koç S, Toplan N, Yildiz K, Toplan H. Effects of mechanical activation on the non-isothermal kinetics of mullite formation from kaolinite. J Therm Anal Calorim. 2011;103:791–6.
26. Wu W, Wu X, Lai S, Liao S. Non-isothermal kinetics of thermal decomposition of $NH_4ZrH(PO_4)_2{\cdot}H_2O$. J Therm Anal Calorim. 2011;104:685–91.
27. Sovizi MR, Anbaz K. Kinetic investigation on thermal decomposition of organophosphorous compounds. J Therm Anal Calorim. 2010;99:593–8.
28. Stefano V, Romolo DR, Carla F. Kinetic study of decomposition for Co(II)- and Ni(II)-1,10-phenanthroline complexes intercalated in c-zirconium phosphate. J Therm Anal Calorim. 2009;97: 805–10.
29. Muraleedharan K, Kanan M, Ganga DT. Thermal decomposition kinetics of potassium iodate. J Therm Anal Calorim. 2011;103: 943–55.
30. Vyazovkin S, Burnham AK, Criado JM, Maqueda LAP, Popescu C, Sbirrazzuoli N. ICTAC Kinetics Committee recommendations for performing kinetic computations on thermal analysis data. Thermochim Acta. 2011;520:1–19.
31. Brown ME, Maciejewski M, Vyazovkin S, Nomen R, Sempere J, Burnham A, Opfermann J, Strey R, Anderson HL, Kemmler A, Keuleers R, Janssens J, Desseyn HO, Li CR, Tang TB, Roduit B, Malek J, Mitsuhashi T. Computational aspects of kinetic analysis Part A: the ICTAC kinetics project-data, methods and results. Thermochim Acta. 2000;355:125–43.
32. Vyazovkin S, Wight CA. Kinetics in solids. Annu Rev Phys Chem. 1997;48:125–49.
33. Gabal MA. Non-isothermal studies for the decomposition course of CdC2O4-ZnC2O4 mixture in air. Thermochim Acta. 2004; 412:55–62.
34. Budrugeac P, Segal E. On the use of Diefallah's composite integralmethod for the non-isothermal kinetic analysis of heterogenous solid-gas reactions. J Therm Anal Calorim. 2005;82:677–80.
35. Arslan H, Külcü N. Thermal decomposition kinetics of anilino-*p*-chlorophenylglyoksime complexes of cobalt(II), nickel(II) and copper(II). Turk J Chem. 2003;27:55–63.
36. Avsar G, Külcü N, Arslan H. Thermal behaviour of copper(II), nickel(II), cobalt(II) and palladium(II) complexes of *N*,*N*-dimethyl-*N*′-benzoylthiourea. Turk J Chem. 2002;26:607–15.
37. Sodhi GS. Correlation of thermal stability with structures for some metal complexes. Thermochim Acta. 1987;120:107–14.